Available online at www.sciencedirect.com
ScienceDirect
Infrared Physics & Technology 50 (2007) 284–290
INFRARED PHYSICS & TECHNOLOGY
www.elsevier.com/locate/infrared

Molecular beam epitaxy growth of HgCdTe for high performance infrared photon detectors

Yong Chang *, C. Fulk, J. Zhao, C.H. Grein, S. Sivananthan

Microphysics Laboratory, Department of Physics, University of Illinois at Chicago, Chicago, IL 60607, USA

Available online 9 November 2006

Abstract

Significant progresses have been made in the molecular beam epitaxy (MBE) growth of HgCdTe for high performance infrared photon detectors with the aid of *in situ* and *ex situ* characterization techniques. Superlattice interfacial layers compensate in part for the influence of non-ideal CdZnTe substrates and hence improved the material quality as well as yield. They result in photoconductive carrier recombination lifetimes approaching theoretical limits set by the intrinsic radiative and Auger recombination mechanisms for 8–14 μm long-wavelength infrared HgCdTe. Very high composition and thickness uniformities have also been achieved. However, the Urbach tail energy, which is associated with structural disorder, was found to be non-uniform for both large wafer (up to $20 \times 20\ mm^2$) and very small area (down to $200 \times 200\ \mu m^2$). After several years of improvements in MBE HgCdTe growth techniques, substrates once again have become a bottleneck to further improvements.

PACS: 81.15.Hi; 81.05.Dz; 71.55.Gs; 72.20.Jv

Keywords: Molecular beam epitaxy; MBE; HgCdTe; Infrared; Photon detector; Material Uniformity

1. Introduction

The narrow gap semiconductor alloy $Hg_{1-x}Cd_xTe$ is the dominant material for the fabrication of high performance infrared photon detectors and detector arrays used in night vision, thermal imaging and ballistic missile defense due in part to its variable direct band gap (through adjusting Cd composition [1]) with a high density of states. Along with the development of HgCdTe, molecular beam epitaxy (MBE) has emerged as a flexible growth technique with a low crystal growth temperature and has been developed to a mature and standard technique to grow sophisticated HgCdTe multilayered crystalline films for the fabrication of infrared detectors with advanced architectures, such as high operation temperature [2,3] multi-color detectors [4,5] or very long wavelength infrared photon detectors [6–8]. These devices typically involve a series of layers of different thickness, bipolar doping concentrations, alloy compositions and even layers with compositional gradients. Device characterization data usually shows that focal plane arrays fabricated from MBE material have much narrower Gaussian-like distributions of device figures of merits than those made from HgCdTe grown by other techniques. Therefore, MBE is expected to be the growth technology of choice for the preparation of the next generation of high performance focal plane array infrared detectors.

2. Experimental

2.1. MBE growth

HgCdTe epilayers were grown on CdZnTe (211)B substrates to ensure the best lattice match. The growth was performed in a Riber 32P MBE system equipped with a valved Hg cell that enables instant adjustments of the Hg flux during growth, reflection-high-energy electron diffraction (RHEED), an infrared pyrometer and *in situ*

* Corresponding author.
E-mail address: yonchang@uic.edu (Y. Chang).

1350-4495/$ - see front matter © 2006 Elsevier B.V. All rights reserved.
doi:10.1016/j.infrared.2006.10.017

spectroscopic ellipsometry (SE). Solid CdTe, Te and elemental Hg were used as source materials for growth. The flux of the CdTe and Te cells was controlled by using different cell temperatures in order to obtain the HgCdTe target composition and growth rate. The Hg flux was controlled by adjusting the corresponding valve and the cell temperature. Before growth, CdZnTe substrates were sequentially degreased with boiled 2-propanol, acetone, methanol, and etched in the 0.5% Br/methanol solution. The substrates were dried using high purity nitrogen gas and carefully mounted between a spring plate and graphite thermal diffusion plates on an indium-free substrate holder. Once introduced into the growth chamber, excessive Te present on the sample surface was removed by heating at 250 °C, followed by annealing at higher temperature under Te flux. RHEED was used to monitor the Te desorption, interface formation, CdTe regrowth, interfacial layer growth and HgCdTe growth. The growth conditions were optimized and maintained in the optimized growth window established previously with our semi-empirical model [9]. Thus, two-dimensional growth of HgCdTe on the CdZnTe substrates takes place from the beginning of nucleation to the end of growth. This growth process also ensured that the samples were almost free of surface defects such as craters [10,11] (also labeled as voids and caused by a non-optimal temperature [12] or as V-shaped defects [13]) and twins. The infrared pyrometer aided in monitoring the growth temperature, and *in situ* spectroscopic ellipsometry was used during all depositions to monitor the substrate temperature before HgCdTe nucleation and to provide composition control during HgCdTe growth. The effective medium approximation (EMA) surface roughness model has been used in the *in situ* SE data fitting to determine the quality of two-dimensional growth during both substrate preparation and HgCdTe growth. A HgTe/CdTe superlattice (SL) interfacial layer has been developed to block substrate roughness as well as prevent threading dislocations from propagating from the CdZnTe substrate to the HgCdTe functional epitaxial layer. During SL interfacial layer growth, the Te and CdTe cell shutters were opened sequentially under fixed Hg flux, resulting in HgTe well layers and barrier layers that were close to pure CdTe, having 0.9–0.95 Cd mole fractions, respectively [14]. The average growth rate of the HgTe layers of the SL was about 0.3–0.4 nm/s, whereas it was 0.1–0.15 nm/s for CdTe layers. A 5 nm/5 nm HgTe/CdTe SL was found to be a reasonable design, allowing the surface roughness to be effectively smoothened while simultaneously reducing the generation of misfit dislocations in HgTe layers that occur when the these layers are too thick. The average growth rate of HgCdTe alloys is 0.6–0.7 nm/s. Note that a constant surface temperature was important to keep the growth conditions within the optimized window and to ensure high uniformity of both crystalline quality and composition. A specially designed, coated sample mounting plate and a temperature ramping recipes were employed to maintain constant surface temperature. Following growth, some samples were annealed for a period of 24 h at 250 °C under a saturated Hg atmosphere to remove Hg vacancies that were generated during MBE growth (since the MBE growth of HgCdTe is intrinsically Te-rich). After growth, the samples were investigated by other *ex situ* characterization methods, including infrared transmission and transmission mapping, etch pit density, X-ray double crystal rocking curves, temperature-dependent Hall effect, photoconductive decay lifetime and fitting, scanning electron microscopy, atomic-force microscopy, TEM, and energy dispersive X-ray (EDX) measurements.

2.2. In situ characterization

SE was used *in situ* to monitor the substrate preparation and MBE growth of HgCdTe. SE characterizes a material's electronic structure as well as its optical properties through variations of its dielectric function, and can be used to determine such quantities as alloy compositions, strains and lattice temperatures. The capability of measuring phase changes gives SE great sensitivity to the presence of thin films on reflecting surfaces, which may be detected to thicknesses of the order of hundredths of monolayers. SE measures the change in polarization of reflected light rather than the intensity. It is extremely sensitive to even small changes in material surfaces and optically accessible interfaces. In the case of a CdTe substrate in a MBE chamber, the measured dielectric function actually is a pseudo-dielectric function that contains contributions from the bulk and from the surface. However, it still gives a reliable relative measure of actual material/surface properties. The non-invasiveness of SE makes it an ideal tool for non-contact *in situ* measurements during MBE growth. These qualities make SE especially useful for the characterization of the surface of the substrate and the study of the near-surface, not yet stabilized, reactive region during the MBE growth. Therefore, it is an extremely valuable *in situ* tool for controlling the MBE growth of HgCdTe. As mentioned, in practice we mainly use *in situ* spectroscopic ellipsometry to monitor the substrate temperature before HgCdTe nucleation and to provide composition control during HgCdTe growth. The effective medium approximation surface roughness model has been employed during *in situ* SE data fitting to determine the quality of two-dimensional growth during both substrate preparation and HgCdTe growth. Some studies have also been conducted on Hg-related absorption and nucleation during MBE growth [15,16].

2.3. Infrared microscope mapping

The composition and thickness uniformity was characterized using FTIR infrared microscope transmission mapping technique. In fact, epitaxial growth, especially MBE growth of HgCdTe, has resulted in improved HgCdTe material uniformity. However, compositional homogeneity has still received attention by the groups engaged in

HgCdTe growth because of the strong dependence of the cutoff wavelength on composition, especially in the long and very long wave infrared bands. To obtain spatial composition and thickness uniformity with reasonably good resolution, many points on the surface of the sample must be inspected by, for example, infrared transmission measurements and a great deal of data must be processed. A computerized homogeneity mapping method can fundamentally simplify measurements and potentially become a routine characterization method that will be helpful in achieving improved material uniformity. Mapping measurements are performed on a Fourier transform infrared spectrometer. For the mapping, the wafer was scanned by a computerized x–y translation stage. The program read the data for processing after the transmission mapping measurements were finished. The thickness was calculated by fitting the interference fringes using an interference matrix method that discussed in detail elsewhere [17]. Initially, a fit to the spectral Fourier transformed data were performed to obtain first guess values of the HgCdTe and CdTe thicknesses. These values were then introduced into the calculation for fitting the untransformed data. The Levenberg–Marquardt [18] method was used for the automatic fitting, and the simulated annealing method [19] was introduced to ensure that the fitting calculation reached the global mean square error (MSE) minimum instead of being trapped by other local MSE minima. The band gap of the layer was defined to be the energy at which the transmission T_r corresponds to an absorption coefficient of $\alpha = 500$ or $1000\ \mathrm{cm}^{-1}$. This point was calculated using the expression $T_r = T_{rmax} \cdot \exp(-\alpha d)$, where T_{rmax} is the average maximum transmission and d is the layer thickness. The composition of the layer was determined at each point from the relationship between x and the band gap given by Hansen et al. [1]. Since the composition x is related to the HgCdTe layer thickness d, and d is related to x, self-consistent fitting calculations were used to obtain x and d simultaneously. After x and d converged to a given precision, e.g. an error in x less than 0.0001 and error in d less than 0.01 μm, the self-consistent fitting calculation is stopped, and reasonably precise values of composition and thickness are obtained. Although the absolute accuracy of x and d values depends on the accuracy of employed formulas, the relative variation value crossing the wafer, which is what the mapping measurements are principally interested in, is of high accuracy. The Urbach tail energy, describing the steepness of Urbach tail of HgCdTe [20,21], was also obtained from the same mapping measurements [22].

2.4. Photoconductive decay lifetime measurement and fitting

The carrier recombination processes in HgCdTe are characterized by recombination lifetimes that are usually measured by fitting photoconductive decay data. The photoconductive decay carrier recombination lifetime was used to characterize the crystalline perfection. The carrier recombination processes in HgCdTe directly contribute to both photon detection and noise generation mechanisms of the corresponding fabricated photovoltaic infrared devices and determine device figures of merit, including detectivities and zero-bias dynamic-resistance-area-products. Auger, radiative and Shockley–Read–Hall (SRH) are three commonly recognized recombination mechanisms. Since the three mechanisms show different temperature dependencies, the measurement of temperature-dependent lifetimes and related fitting calculations are therefore helpful to separate the contributions from each mechanism and offer an approach to study the recombination processes in HgCdTe. Among the three mechanisms, Auger and the radiative recombination are intrinsic, and are consequently determined by intrinsic material properties, such as composition and doping levels that can be precisely measured by other techniques e.g. Hall effect and infrared absorption mapping [17]. The calculation of lifetimes determined by intrinsic Auger and radiative recombination mechanisms in this work used sets of semi-empirical formulas based on Kane's $\mathbf{k} \cdot \mathbf{p}$ model with several key parameters determined experimentally [23]. These intrinsic mechanisms establish the theoretical lifetime upper limits. The differences between the calculated and measured lifetime values are attributed to SRH recombination, which arises from impurities or defects in HgCdTe. Thus, characterizing SRH centers and trying to increase SRH lifetimes is the ultimate goal for most HgCdTe growers. The lifetime fitting procedure and models were carefully characterized and improved to clearly identify SRH lifetimes. The Levenberg–Marquardt method, which combines the advantages of the steepest decent method and Newton's method, was employed to automatically fit the temperature dependent lifetime data so as to precisely extract information related to SRH carrier recombination processes. Hessian matrices of the model were used to analyze the fitting certainties. We found that the fitting parameters can be trapped in local minima, strongly correlating with starting values. Therefore, the Monte Carlo and simulated annealing methods were employed to help the program converge to the global minimum. Additionally, low temperature points were weighted more heavily in order to obtain more precise SRH energy levels. Constrains were used to ensure that the fitting calculations are capable of giving only physically reasonable results. Based on the above methods, carrier recombination lifetime measurements were developed as a routine characterization technique in our laboratory. They were used to help improve the material quality by optimizing growth condition, substrate preparation and post-growth thermal processing procedures.

3. Results and discussion

Current growth techniques for producing CdZnTe bulk substrates are not ideal. Several different types of defects often exist on the surfaces of commercially available substrates and are likely to cause defects in HgCdTe epilayers

grown by MBE [24]. They include small-angle crystal boundaries as observed by X-ray topographic mapping. Typical topographical features of commercial CdZnTe substrates are discussed in Refs. [24,25]. It has been demonstrated that all substrate defects are likely to be transferred directly to HgCdTe epilayers if no effective interfacial layers are present, as shown in Fig. 1. These defects lead to a high density of threading dislocation and short defect-mediated carrier recombination [26]. An additional problem is that the compositional uniformity of these substrates is poor due to limitations of bulk growth techniques. For example, a typical commercial specification for the Zn composition of a CdZnTe substrate is 0.035 ± 0.01, which corresponds to a considerable variation in the lattice constant of the material. The lattice constant is not always uniform across the surface either for a given substrate or from one substrate to another. Damage due to polishing may be present, which will tend to create a microscopically rough substrate surface after pre-growth treatment. Threading dislocations also occur, as revealed by etch pit density (EPD) studies. A typical EPD value is 10^4 cm^{-2} using Everson's etchant [27], although this number may vary substantially from substrate to substrate and even from area to area on the same substrate. Te precipitates have also been reported on substrate surfaces. Indeed, the density of these precipitates has been found to be the lowest limitation on the void defect density [28] that can be explained by a Te_2 molecular flux directly nucleated on solid Te [9].

To improve the MBE HgCdTe growth yield, grown material properties and reproducibility, we researched, developed and employed HgTe/CdTe SL interfacial layers. Electron microscopic observations confirmed that a SL interfacial layer is capable of not only smoothing out the initial substrate surface roughness during MBE growth but also bending threading dislocations. Such bending forces three-dimensional dislocations to move/glide in a two-dimensional interfacial plane, which offers a much higher chance for them to glide into a reaction distance and merge together, greatly reducing the possibility of dislocations propagating into the HgCdTe device functional layers to improve material properties [29]. By taking advantage of SL interfacial layers, EPDs in the low 10^5 cm^{-3} range, which are widely recognized to be good enough for the fabrication of typical focal plane infrared detector arrays, have been reproducibly achieved. Photoconductive decay lifetime measurements showed that the lifetime values approached theoretical limits as determined by intrinsic recombination mechanisms. The influences of

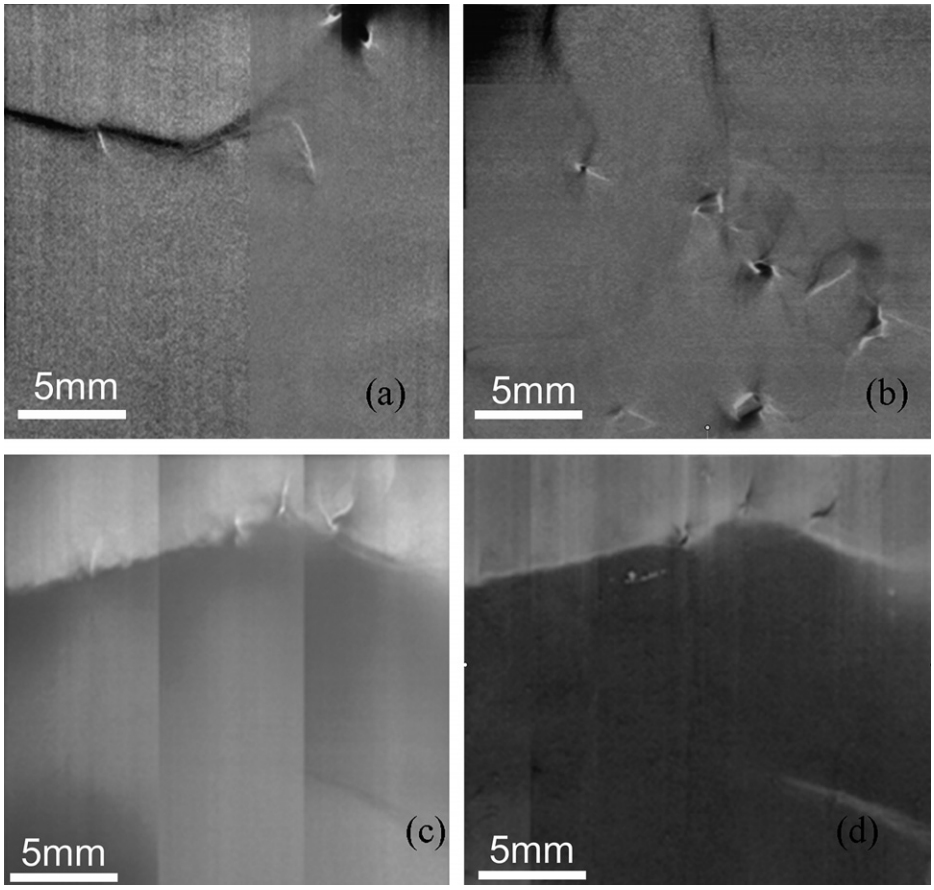

Fig. 1. (a)–(c): X-ray topographic mapping measurement results from a commercially purchased 20 mm × 20 mm CdZnTe wafer ((a)–(c) after Ref. [24]); (d) X-ray topographic mapping results of HgCdTe film grown on (c) without the interfacial layer described in this paper, which shows that almost all substrate crystalline imperfections were transferred to the HgCdTe MBE film.

the SRH recombination mechanism are greatly reduced to the point of being negligible. An excellent EPD value in the mid-10^4 cm^{-2} was reached in a LWIR HgCdTe sample. The details of growth as well as the operating mechanisms of these SL interfacial layers have been discussed elsewhere in detail [30]. High quality HgCdTe materials approaching theoretical lifetime limits were obtained with the aid of these efforts.

After growth, typical HgCdTe grown inside the optimized growth window shows high composition and thickness uniformity perpendicular to the growth direction, as measured by Fourier transform infrared microscope mapping and shown in Fig. 2. For this sample, the average composition x is 0.2182 with a standard deviation Δx of 0.0006. Higher composition material is found in about 2×2 mm^2 areas near the corners. The HgCdTe layer was also found to be thicker in the center, being especially thin in the corners (where the composition is higher). The growth temperature in the corners is expected to be a bit high due to the relatively low thermal conductivity of CdZnTe, so the radiative thermal energy absorbed by HgCdTe on the CdZnTe near a corner cannot be easily transferred out, as confirmed by finite element analyses. The slightly higher temperature leads to a decrease in the Hg sticking coefficient [31], which induces a higher Cd composition and thinner material in the corners than that in the center, according to MBE growth thermodynamic kinetic analysis [32,33]. Under certain conditions, a non-uniformly distributed flux could in principle also result in such patterns. We also performed measurement for MBE grown HgCdTe on 3-in. Si substrate using CdTe buffer layers in the same MBE chamber. The very good composition and thickness uniformities in the 20×20 mm^2 area of the wafer center, as shown in Table 1, clearly excludes that possibility. Considering the high thermal conductivity of Si and the relatively large area of the grown epilayer, the large area nonuniformity can be attributed to a nonuniformly distributed flux; however, the result shows that the flux is very uniform in the central area. Hence the nonuniformity in the substrate temperature distribution must have stemmed almost solely from the substrate geometry. The conclusion that higher growth temperatures are present in the corners can also be deduced from the differences observed between surface defects in the center and those in the corners of some of our samples, e.g. the size and density of crater defects, which are closely related to the growth temperature [20]. The average thickness of the sample is 7.84 μm with a standard deviation Δd of 0.03 μm. The large nonuniformity of composition and thickness mainly exists in small areas near the sample corners.

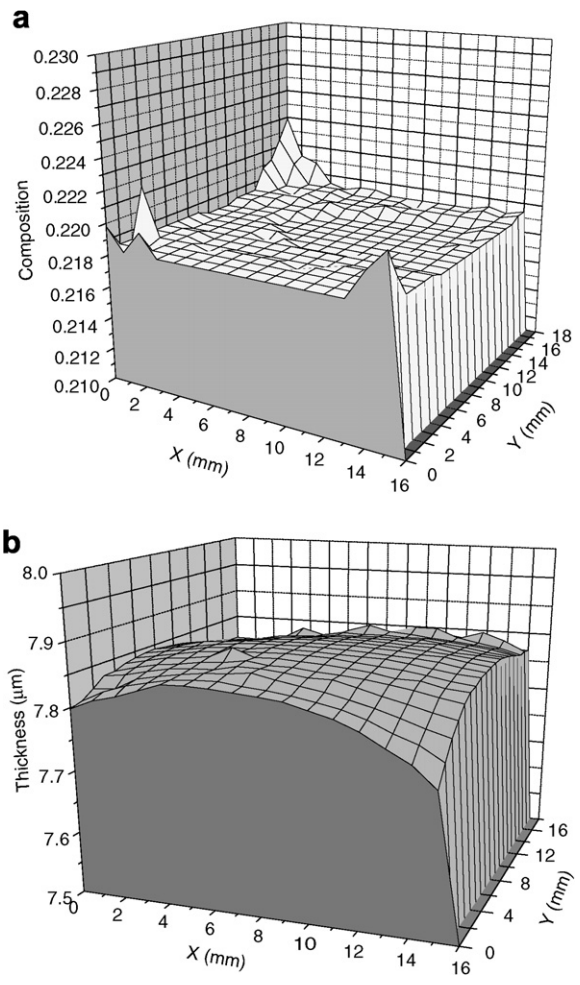

Fig. 2. Mapping results for a HgCdTe sample grown by MBE on a CdZnTe substrate. (a) Composition, and (b) HgCdTe thickness.

In addition to the macroscopic uniformity of MBE-grown HgCdTe wafers, microscopic uniformity has also attracted attention since it is suspected of causing nonuniformities in the performance figures of merit (e.g. quantum efficiencies, dark currents, detectivities) of IRFPAs [34]. MBE-grown long-wavelength-infrared HgCdTe materials were also investigated using infrared microscope mapping. A 20 μm × 20 μm focused infrared beam was employed to study the microscopic uniformity of MBE-grown HgCdTe over areas of 200 μm × 200 μm, in contrast to the 100 μm diameter beam used for macroscopic uniformity measurements. The integration times or scanning times were found to be of great importance to obtaining reliable measurements because the beam signal is relatively weak comparing with typical spectroscopic measurement. We found that the measured standard deviation becomes stable only when the scan number increases above 32, at which point the standard deviation is only determined by the material

Table 1
Typical composition and thickness uniformity data of 3-in. MBE-grown HgCdTe on Si

	Composition	Standard deviation	Thickness (μm)	Standard deviation (μm)
Total 3-in. area	0.2340	±0.0042	7.15	±0.07
Central 20×20 mm area	0.2299	±0.0008	7.21	±0.01

itself. A best relative compositional uniformity of <0.0001 over an area was obtained, as shown in Fig. 3a. The standard deviation of the relative thickness of the MBE layer is less than 0.002 μm over the corresponding area, as shown in Fig. 3b. Again, a larger microscopic deviation in both composition and thickness can only be found near the edges or corners of the MBE-grown HgCdTe wafers, corresponding to the macroscopic non-uniformities caused by the edge effects of the MBE heating plate.

We also performed mapping measurements of the Urbach tail energy. We found, that the standard deviation of the Urbach tail energy over both the macroscopic and microscopic areas is not uniform. For example, for the 200 μm × 200 μm area, the standard deviation is as high as 0.36 meV, which is non-uniformly distributed, as shown in Fig. 3c.

The Urbach tail energy, dominated by contributions from electron–phonon interactions, alloy disorder and structural disorder, was found to be capable of characterizing material quality [17]. We noticed that those samples with surface microtwin defects that correlate with low growth temperatures and with high dislocation densities always showed relatively high Urbach tail energies. However, when the growth is controlled in the optimized growth window and the material quality is very good, we still can find that the Urbach tail energy distribution is not uniform. We also find that the Urbach tail energy has a large standard deviation over a small area, which suggests that non-uniformly distributed structural disorder dominates the nonuniformity of device performance figures of merit in HgCdTe IRFPAs. Most likely, the structural disorder is simply copied from the non-ideal CdZnTe substrate. Due to further improvements in MBE growth techniques, the substrate once again has emerged as a bottleneck to the enhancement of MBE growth of high quality HgCdTe.

4. Summary and future directions

Great progress has been made in the MBE growth of HgCdTe for high performance infrared photon detectors. *In situ* techniques, especially SE, has dramatically enhanced the capability of maintaining growth in the optimized window and improving uniformity along the growth direction. SL interfacial layers compensate in part for non-ideal CdZnTe substrates and hence improve material quality and yield. Photoconductive lifetime measurements and fittings reveal the dominant recombination mechanisms inside the grown epilayers and offer feedback to MBE growers to optimize the growth conditions. Very high composition and thickness uniformities have been achieved. However, the Urbach tail energy, which is closely correlated with

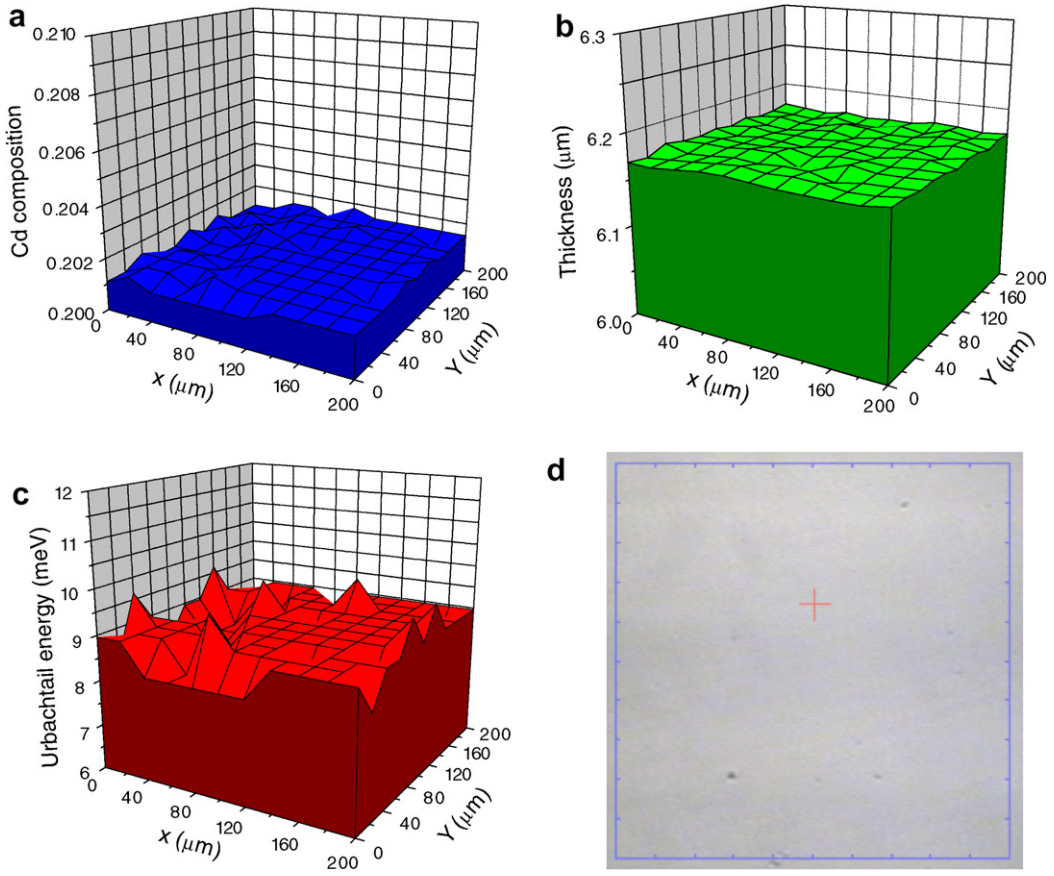

Fig. 3. Composition, thickness and Urbach tail mapping results as well as a surface morphology photograph of a 200 μm × 200 μm area of a LWIR MBE HgCdTe sample. (a) Composition; (b) thickness; (c) Urbach tail energy; and (d) the surface morphology picture of the same scanned area.

structural disorder, is found to be non-uniform over not only macroscopic but also microscopic scales. Structural disorder is probably associated with non-ideal substrates. After several years of improvement of MBE growth itself, substrates have again become an issue.

To further improve the quality and yield of MBE grown HgCdTe in addition to improving CdZnTe substrates, another approach is to focus on Si substrates with optimized buffer layers. MBE growth technology for HgCdTe on Si has already reached a mature stage for mid-wavelength infrared (3–5 μm cutoff) detectors. Here, the anticipated progress is principally in the areas of incremental optimization of the growth parameters and streamlining of the process for mass production. Applications in the 8–14 μm long wavelength infrared and very long wavelength infrared regions are still a challenge because of the high dislocation densities associated with the use of Si substrates, up to 10^6 cm^{-2} [35]. An extra advantage of developing Si-based substrates is that they can directly lead to the realization of multicolor, monolithic focal plane arrays. Although a monolithic linear array of detectors has already been demonstrated [36], the integration of a two-dimensional array on a Si-based readout circuit has yet to be achieved. Radical improvements in the quality of the HgCdTe/CdTe/Si layers are necessary. They require new ways to overcome the large lattice and thermal mismatches between CdTe and Si. To this end, our laboratory is currently exploring the viability of growing CdTe on pattered as well as malleable substrates. Such substrates are presently available in the market and include very thin layers ($\sim$ 50 Å) of Si bonded on SiO_2/Si wafers. Another form of compliant substrate that is under study is a twist-bonded substrate. In this case, a very thin Si layer is bonded to a silicon wafer with a slight rotation angle. This form of bonding produces a regular network of dislocations surrounding pristine areas of silicon, the size of which is of the order of several nm^2. It is hoped that growth on such substrates will accommodate the lattice mismatch, resulting in near dislocation-free CdTe and HgCdTe.

References

[1] G.L. Hansen, J.L. Schmit, T.N. Casselman, J. Appl. Phys. 53 (1982) 7099.

[2] W.E. Tennant, S. Cabelli, K. Spariosu, J. Electron. Mater. 28 (1999) 582.

[3] T.J. de Lyon, J.E. Jensen, I. Kasai, G.M. Venzor, K. Kosai, J.B. de Bruin, W.L. Ahlgren, J. Electron. Mater. 31 (2002) 220.

[4] L.A. Almeida, M. Thomas, W. Larsen, K. Spariosu, D.D. Edwall, J.D. Benson, W. Mason, A.J. Stoltz, J.H. Dinan, J. Electron. Mater. 31 (2002) 669.

[5] E.P.G. Smith, L.T. Pham, G.M. Venzor, E.M. Norton, M.D. Newton, P.M. Goetz, V.K. Randall, A.M. Gallagher, G.K. Pierce, E.A. Patten, R.A. Coussa, K. Kosai, W.A. Radford, L.M. Giegerich, J.M. Edwards, S.M. Johnson, S.T. Baur, J.A. Roth, B. Nosho, T.J. De Lyon, J.E. Jensen, R.E. Longshore, J. Electron. Mater. 33 (2004) 509.

[6] A.I. D'Souza, R.E. DeWames, P.S. Wijewarnasuriya, G. Hildebrandt, J.M. Arias, J. Electron. Mater. 30 (2001) 585.

[7] Y.D. Zhou, C.R. Becker, Y. Selamet, Y. Chang, R. Ashokan, R.T. Boreiko, T. Aoki, D.J. Smith, A.L. Betz, S. Sivananthan, J. Electron. Mater. 32 (2003) 608.

[8] M.B. Reine, S.P. Tobin, P.W. Norton, P. LoVecchio, Proc. SPIE 5795 (2005) 211.

[9] Y. Chang, G. Badano, J. Zhao, C.H. Grein, S. Sivananthan, T. Aoki, D.J. Smith, Appl. Phys. Lett. 83 (2003) 4785.

[10] T. Aoki, D.J. Smith, Y. Chang, J. Zhao, G. Badano, C. Grein, S. Sivananthan, Appl. Phys. Lett. 82 (2003) 2275.

[11] T. Aoki, Y. Chang, G. Badano, J. Zhao, C. Grein, S. Sivananthan, D.J. Smith, J. Cryst. Growth 265 (2004) 224.

[12] L. Chen, Y. Wu, M.F. Yu, S.L. Wang, Y.M. Qiao, L. He, J. Infrared Millim. Waves 20 (2001) 406.

[13] I.V. Sabinina, A.K. Gutakovsky, Y.G. Sidorov, A.V. Latyshev, J. Cryst. Growth 274 (2005) 339.

[14] Y. Selamet, Y.D. Zhou, J. Zhao, Y. Chang, C.R. Becker, R. Ashokan, C.H. Grein, S. Sivananthan, J. Electron. Mater. 33 (2004) 503.

[15] G. Badano, Y. Chang, J.W. Garland, S. Sivananthan, Appl. Phys. Lett. 83 (2003) 2324.

[16] G. Badano, Y. Chang, J.W. Garland, S. Sivananthan, J. Electron. Mater. 33 (2004) 583.

[17] Y. Chang, G. Badano, E. Jiang, J.W. Garland, J. Zhao, C.H. Grein, S. Sivananthan, J. Cryst. Growth 277 (2005) 78.

[18] W.H. Press, S.A. Teukolsky, W.T. Vetterling, B.P. Flannery, Numerical Recipes in C, Cambridge University Press, Cambridge, 1995, p. 683.

[19] W.H. Press, S.A. Teukolsky, W.T. Vetterling, B.P. Flannery, Numerical Recipes in C, Cambridge University Press, Cambridge, 1995, p. 444.

[20] Y. Chang, G. Badano, J. Zhao, Y.D. Zhou, R. Ashokan, C.H. Grein, V. Nathan, J. Electron. Mater. 33 (2004) 709.

[21] Y. Chang, C.H. Grein, S. Sivananthan, M.E. Flatte, V. Nathan, S. Guha, Appl. Phys. Lett. 89 (2006) 062109.

[22] Y. Chang, G. Badano, E. Jiang, J. Zhao, Y.D. Zhou, C.H. Grein, S. Sivananthan, Composition, thickness and Urbach slope distribution of HgCdTe MBE wafers by infrared microscope mapping, in: 2002 US Workshop on Physics and Chemistry of II–VI Materials, San Diego, CA, 2002.

[23] See, for example, V.C. Lopes, A.J. Syllaios, M.C. Chen, Semicond. Sci. Technol. 8 (1993) 824, and the references cited therein.

[24] H. Abad, J. Zhao, G. Badano, Y. Chang, S. Sivananthan, in: Military Sensing Symposia, 22–26 March 2004, Tucson, AZ, USA.

[25] G.A. Carini, C. Arnone, A.E. Bolotnikov, G.S. Camarda, R. DeWames, J.H. Dinan, J.K. Markunas, B. Raghothamachar, S. Sivananthan, R. Smith, J. Zhao, Z. Zhong, R.B. James, J. Electron. Mater. 35 (2006) 1495.

[26] J. Zhao, Y. Chang, G. Badano, S. Sivananthan, J. Markunas, S. Lewis, J.H. Dinan, P.S. Wijewarnasuria, Y. Chen, G. Brill, N. Dhar, J. Electron. Mater. 33 (2004) 881.

[27] W.J. Everson, C.K. Ard, J.L. Sepich, B.E. Dean, G.T. Neugebauer, J. Electron. Mater. 24 (5) (1995) 505.

[28] E.C. Piquette, M. Zandian, D.D. Edwall, J.M. Arias, J. Electron. Mater. 30 (2001) 627.

[29] Y. Chang, J. Zhao, H. Abad, C.H. Grein, S. Sivananthan, T. Aoki, D.J. Smith, Appl. Phys. Lett. 86 (2005) 131924.

[30] Y. Chang, C.H. Grein, J. Zhao, S. Sivananthan, C.Z. Wang, T. Aoki, D.J. Smith, P.S. Wijewarnasuriya, V. Nathan, J. Appl. Phys., in press.

[31] S. Sivananthan, X. Chu, J. Reno, J.P. Faurie, J. Appl. Phys. 60 (1986) 1359.

[32] J.P. Gailliard, Revue. Phys. Appl. 22 (1987) 457.

[33] T. Colin, T. Skauli, J. Electron. Mater. 26 (1997) 688.

[34] J.D. Phillips et al., Appl. Phys. Lett. 83 (2003) 3701.

[35] P. Boieriu, C.H. Grein, S. Velicu, J. Garland, C. Fulk, S. Sivananthan, A. Stoltz, L. Bubulac, J.H. Dinan, Appl. Phys. Lett. 88 (2006) 062106.

[36] S. Velicu, T.S. Lee, R. Ashokan, C.H. Grein, P. Boieriu, Y.P. Chen, J.H. Dinan, D. Lianos, SPIE Proc. 5209 (2003).